Biosensors and Bioelectronics 51 (2014) 413–420

Contents lists available at ScienceDirect

Biosensors and Bioelectronics

journal homepage: www.elsevier.com/locate/bios

Application of ZnO/graphene and S6 aptamers for sensitive photoelectrochemical detection of SK-BR-3 breast cancer cells based on a disposable indium tin oxide device

Fang Liu [a], Yan Zhang [a], Jinghua Yu [a,*], Shaowei Wang [a], Shenguang Ge [b], Xianrang Song [c]

[a] Key Laboratory of Chemical Sensing & Analysis in Universities of Shandong, School of Chemistry and Chemical Engineering, University of Jinan, Jinan 250022, PR China
[b] Shandong Provincial Key Laboratory of Preparation and Measurement of Building Materials, University of Jinan, Jinan 250022, PR China
[c] Cancer Research Center, Shandong Tumor Hospital, Jinan 250012, PR China

ARTICLE INFO

Article history:
Received 28 May 2013
Received in revised form
8 July 2013
Accepted 31 July 2013
Available online 22 August 2013

Keywords:
Photoelectrochemical biosensor
ZnO/graphene
S6 aptamers
SK-BR-3 cancer cells
Indium tin oxide device

ABSTRACT

ZnO/graphene (ZnO/G) composite and S6 aptamer were employed to sensitive photoelectrochemical (PEC) strategy for the specific detection of SK-BR-3 cancer cells based on a portable indium tin oxide microdevice. ZnO/G composite was synthesized using a facile ultrasonic method, and then applied to improve the PEC performance due to the unique hollow structure of ZnO naospheres and the superior properties of graphene. Subsequently, S6 aptamer was applied to this specific detection of SK-BR-3 cancer cells. And the concentration of SK-BR-3 cells was measured with a low detection limit of 58 cells mL^{-1} and a wide linear range of $1 \times 10^2 - 1 \times 10^6$ cells mL^{-1}, through the decrease in photocurrent intensity resulting from the increase in steric hindrances when specifically recognized with S6 aptamers. Excellent discrimination against target and analogous cells was demonstrated, indicating the high selectivity of the proposed cell sensor. Our work also demonstrated a sensitive, stable and low cytotoxicity approach for early and accurate detection of cancer cells.

© 2013 Elsevier B.V. All rights reserved.

1. Introduction

Cancer and its metastasis with malignant cancer cells spreading to distant sites is a leading cause of mortality and despite advances in early detection and treatment, patients continue to suffer from the disease (Krishnamurthy et al., 2010; Pantel et al., 2008). Rapid selective detection of cancer cells is an important challenge for the diagnosis and treatment of tumors (Faenza et al., 2012; Nam et al., 2009). Target cell-specific aptamers have the potential to serve as molecular probes for specific recognition of the cancerous cells from complex mixtures (King et al., 2009; Chen et al., 2009a, 2009b). A well-characterized breast cancer cell line, SK-BR-3, which overexpresses the epithermal growth factor receptor HER2/c-erb-2/Neu (HER2) on the cell surface, has been used to demonstrate the ultrasensitive detection capability. And S6 RNA aptamer showed strong affinity to SK-BR-3, but not to MCF-7, HER-2-underexpressing cancer cell line, so it was selected to specifically recognize the SK-BR-3 cell.

Some recent works in fluorescent imaging for cancer detection have been reported (Yang et al., 2010a, 2011, 2012; Zhang et al., 2011; Hu et al., 2012; Robinson et al., 2011; Markovic et al., 2011; Akhavan et al., 2012a; Akhavan and Ghaderia, 2013), but they do have some disadvantages, such as high price and complex operation. As a photo-voltaic conversion method, photoelectrochemical (PEC) detection represents a newly emerged but dynamically developing analysis technique (Zhao et al., 2012; Li et al., 2012), which has attracted substantial research scrutiny for its desirable sensitivity and hence better analytical performances. In bioassay, taking advantage of the photoactive transducers, the PEC bioassay system converts the specific biorecognition events into the photocurrent signal, providing an elegant route for probing various biorecognition reactions. And, to further improve the PEC detection sensitivity, composites have been researched recently.

ZnO has been researched intensively as practically applicable materials in photocatalysis and photovoltaic cells, because of its suitable band gaps, stability against photocorrosion, high photoelectric and photocatalytic activities (Meng et al., 2013; Zhang et al., 2008). However, the quick recombination of photogenerated charge carriers has significantly decreased the photocatalytic performance of ZnO in aqueous solution. Currently a particularly attractive option is to design and develop hybrid materials based on ZnO to solve this problem (Cho et al., 2010; Zhang et al., 2009). As we all know, graphene shows excellent ability in electrochemical sensing of biomaterials (Akhavan et al., 2012b). And in the

* Corresponding author. Tel.: +86 531 82767161; fax: +86 531 82765969.
E-mail addresses: ujn.yujh@gmail.com, 306375767@qq.com (J. Yu).

0956-5663/$ - see front matter © 2013 Elsevier B.V. All rights reserved.
http://dx.doi.org/10.1016/j.bios.2013.07.066

photocatalysis process, graphene can act as an excellent electron-acceptor/transport material to effectively facilitate the migration of photoinduced electrons and hinder the charge recombination in the electron-transfer processes due to the electronic interaction between ZnO and graphene (Tian et al., 2012; Akhavan (2011)). Despite numerous methods have been developed for the synthesis of ZnO/G hybrid materials to date (Kavitha et al., 2012; Wu et al., 2012; Liu et al., 2011), the exploration on ZnO/G composite is not nearly enough so far. In this work, the synthesis of ZnO/G composite was carried out through a pre-processed stock solution and a facile ultrasonication process. And the prepared ZnO/G composite exhibited an improved photocurrent performance, due to the unique hollow structure of ZnO naospheres and the superior properties of graphene.

Recently indium tin oxide (ITO) based devices is introduced for PEC application due to their low-cost and ease of use (Shen et al., 2011). And screen printed electrodes (SPEs)-based devices (Metters et al., 2011) are applied as promising technology for conventional commercial three-electrode system because of their portability and low consumption of reagents/samples. Inspired by Stefano et al. (Stefano et al., 2007) and Chen et al. (Chen et al., 2009a, 2009b), herein we fabricated an ITO-based SPEs device with acid etch treatment for PEC application.

Herein, we described the construction of a competitive PEC biosensor for precise counting of SK-BR-3 cancer cells based on a portable ITO three-electrode device fabricated by acid etching with screen printed technique. ZnO/G composite was synthesized and drop-cast onto the ITO working electrode (WE) as PEC sensing platform to improve the PEC performance. And Au nanoparticals (AuNPs) were electrodeposited on ZnO/G composite to immobilize amino modified S6 aptamers. Then SK-BR-3 cancer cells were specially recognized with S6 aptamers. As the supporting electrolyte for photocurrent measurements, ascorbic acid (AA) was exploited as an efficient and nontoxic electron donor for scavenging photogenerated holes under mild solution medium. And, the PEC reaction was triggered under the irradiation of ultraviolet light at room temperature.

2. Methods

2.1. Synthesis of ZnO/G composite

Experimentally, 10 mL of graphene oxide (GO, detail synthesis can be found in the supplemental material) (5 mg mL^{-1}) was heated to 98 °C under stirring for appropriate time to obtain a condensed solution with 3 mL, and then cooled down to 65 °C to produce a ropy stock solution. 1.2 g hydrated zinc acetate ($Zn(Ac)_2 \cdot 2H_2O$) was added to 25 mL dimethyl sulfoxide (DMSO) under stirring, and heated to 50 °C. Then the stock solution was added to the above $Zn(Ac)_2$ solution. Subsquently, ultrasonication was performed on the mixture by an ultrasonic apparatus (Sonics: VCX-900 W, 50% amplitude) for 30 min (15 s on and 5 s off).

2.2. Fabrication of PEC biosensor for cancer cells

The fabrication procedure of the PEC biosensor for SK-BR-3 breast cancer cells was illustrated in Scheme 1. ITO devices (the fabrication process of the ITO device can be seen in supplemental material) were sonicated in acetone, ethanol, and water for 15 min each. Then, 0.4 g of ZnO/G powder was dispersed ultrasonically in 10 mL of water, and 10 uL of the resulting colloidal dispersion (0.04 g mL^{-1}) was drop-cast onto ITO working electrode (WE) with a diameter. After drying in air, the film was sintered at 450 °C for 30 min in air to improve the contact between the film and the substrate. It was then naturally cooled to room temperature. The ZnO/G composite coated ITO WE was referred as a ZnO/G/ITO electrode. Then, AuNPs were electrodeposited on the ZnO/G/ITO electrode surface by droppinging 10 μL 1% chloroauric acid ($HAuCl_4 \cdot 4H_2O$) on the electrode and exerting the potential of −0.2 V for 30 s to obtain AuNPs dotted ZnO/G/ITO electrode, followed by washing with pH 7.4 PBS. After that, 10 μL 10^{-6} M animo modified S6 aptamers were dropped on the electrode for 1 h to bond with AuNPs, followed by dropping 1% bovine serum albumin (BSA) to block the uncovered electrode surface.

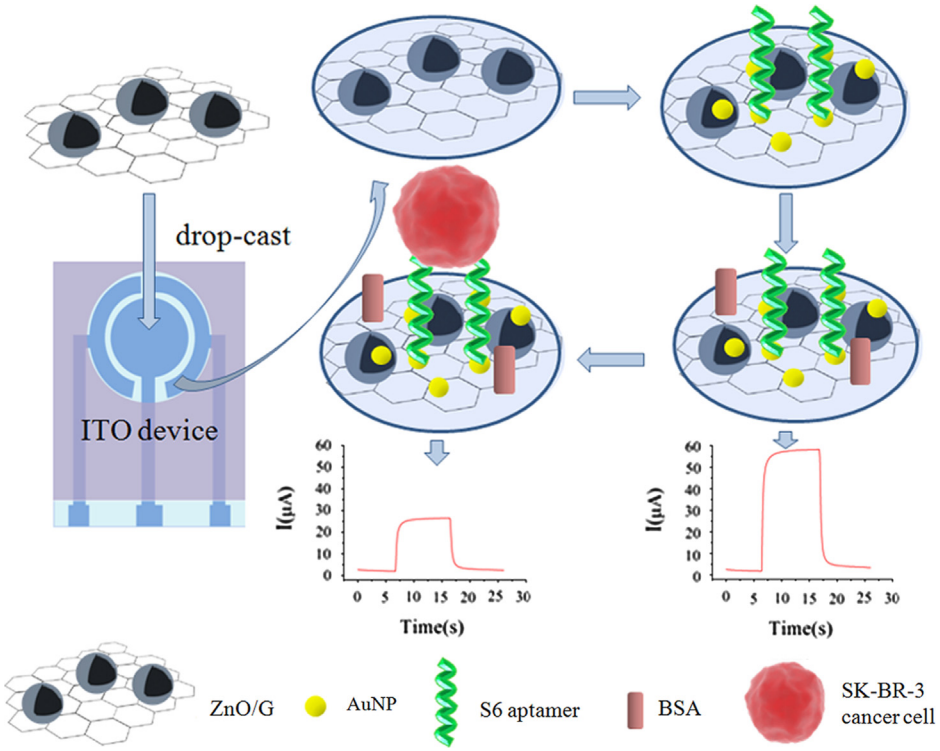

Scheme 1. Schematic representation of the fabrication of the PEC cell sensor based on S6 aptamers-AuNPs dotted ZnO/G modified ITO WE.

2.3. PEC measurement

After washing with water, 10 μL of PBS containing different numbers of SK-BR-3 cancer cells were dropped on the modified ITO WE to hybridize with S6 aptamers at 37 °C for 50 min, and then washed with PBS. After that, 20 μL of AA (0.1 M in pH 7.4 PBS) was added onto the electrode and the PEC measurements were performed. PEC signals related to the cell concentrations could be measured at an applied potential of 0 V with UV light irradiation.

3. Results and discussion

3.1. Characterization of synthesized nanomaterials

3.1.1. SEM, TEM characterization and XRD analysis

The morphologies of ZnO nanospheres, ZnO/G composites and AuNPs dotted ZnO/G were characterized by scanning electron microscope (SEM) (Fig. 1). The hollow structure of ZnO nanosphere was displayed in Fig. 1A with diameter of about 300 nm. Clearly, the stratiform graphene covered with ZnO hollow spheres was observed, as shown in Fig. 1B. On the other hand, the stratiform graphene can also act as a substrate for ZnO nanospheres and it was observed that when no GO was added in the synthesis, the large ZnO consisting of aggregated ZnO nanospheres were obtained. The TEM image (Fig. 1C) further showed that the ZnO nanospheres with apparent hollow structure were assembled on the wafery graphene. From Fig. 1D, it can be seen that AuNPs were electrodeposited on the ZnO/G modified ITO WE uniformly to immobilize S6 aptamers.

The IR spectra of GO, ZnO and ZnO/G composite were shown in Fig. 1E. The broad absorption peaks at 1056, 1228 and 1724 cm^{-1} are attributed to the characteristic stretching vibration of C–O, and C=O of COOH groups situated at the edges of GO sheets, respectively. But for the ZnO/G prepared via ultrasonic reaction, the three absorption peaks decrease dramatically in intensity. The result indicates that the GO has been reduced to a great extent. Furthermore, the absorption band at 500 cm^{-1} for the ZnO/G can be assigned to the stretching vibration of Zn–O, which is red-shifted of ZnO. The blue shift probably results from the coordination among

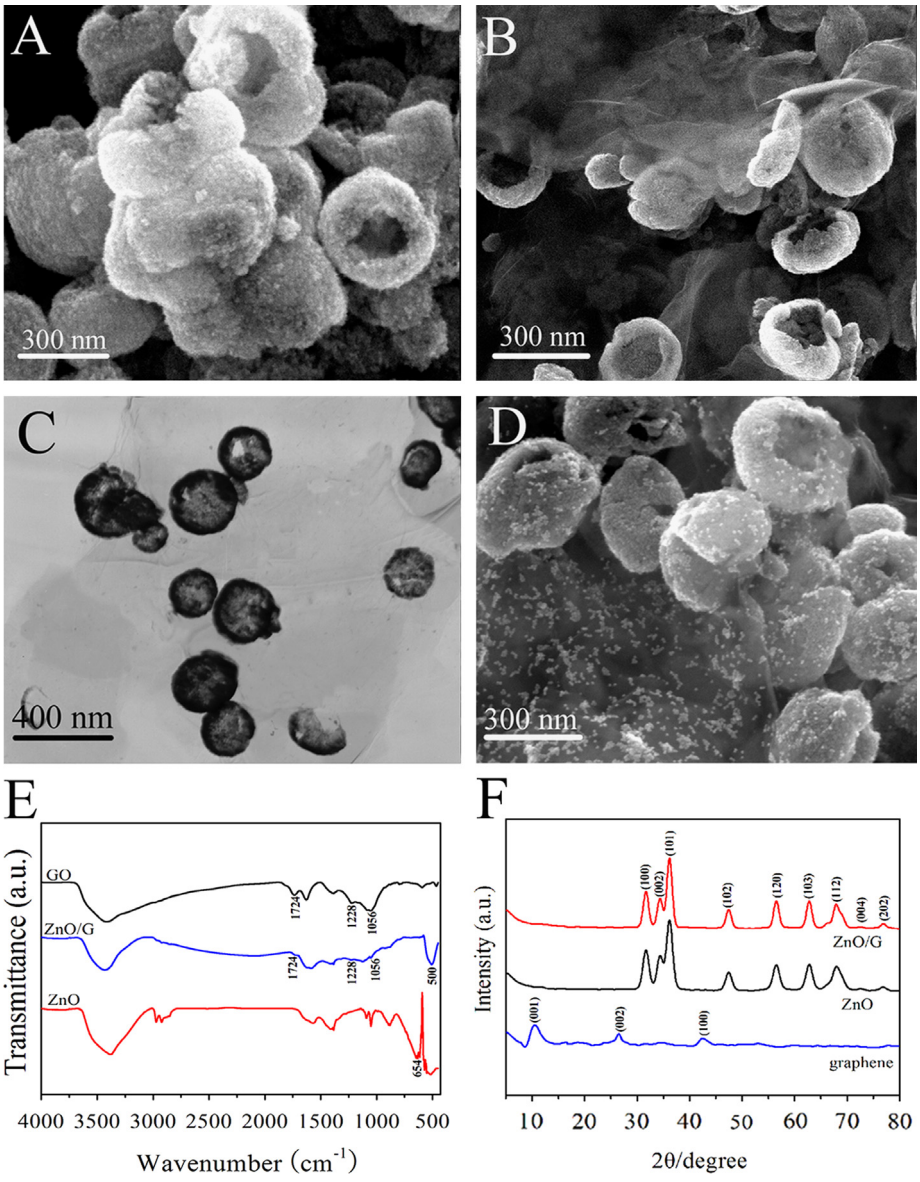

Fig. 1. SEM images of ZnO nanospheres (A), ZnO/G composites (B) and AuNPs dotted ZnO/G (D); TEM image of ZnO/G composites (C); IR spectra (E) and XRD patterns (F) of graphene, ZnO nanospheres and ZnO/G composites.

the residual hydroxyl, epoxy groups on the graphene sheets and ZnO hollow spheres.

The powder X-ray diffraction (XRD) patterns of graphene, ZnO and ZnO/G were shown in Fig. 1F. Graphene exhibited a strong (001) diffraction peak at 10.2°, a (002) peak at 26° and a (100) peak at 44.5° (Tang et al., 2009). The XRD analysis further showed that the main diffraction peaks of ZnO/G composite were similar to that of pure ZnO and corresponds to wurtzite-structured ZnO (JPCDS 36-1451), which indicated that the presence of graphene did not result in the development of new crystal orientations or changes in preferential orientations of ZnO. No typical diffraction peaks of carbon species were observed, which was due to the low amount of graphene in the composite (Chen et al., 2011).

3.1.2. *Raman spectra and X-ray photoelectron spectra (XPS) of ZnO/G composite*

Raman is an important tool to investigate the structure of nanomaterials, especially for the verification of carbon materials. As reported, the peak located at the low frequency ($\sim$ 440 cm^{-1}) is assigned to the ZnO nonpolar optical phonons (Luo et al., 2012). This peak shifts to lower frequency (428 cm^{-1}) due to the interaction of ZnO and graphene sheets. The Raman spectra (Fig. 2A) of ZnO/G composite shows two characteristic bands: the G band (1580 cm^{-1}) and the D band (1350 cm^{-1}). The peak at 2700 cm^{-1} associates with the 2D band. It was shown that the G band of the single-layer graphene, located at 1585 cm^{-1}, shifts about 5 cm^{-1} into lower wavenumbers after stacking 2–6 graphene layers (Ferrari et al., 2006). The 2D band of the single-layer graphene sheets is usually observed at 2679 cm^{-1}, while for the multilayers (2–4 layers) it shifts to higher wavenumbers by 21 cm^{-1}. The nearly asymmetrical shape of the peak also confirmed the presence of both single- and multilayer graphene sheets in the samples (Akhavan, 2010; Calizo et al., 2007; Kudin et al., 2008; Kim et al., 2009).

To obtain the Zn/C and O/C ratios, XPS was used in this regard. As can be observed in Fig. 2B, we can see that the XPS spectrum of C1s can be deconvoluted into two peaks centered at 284.7 and 288.8 eV. The peak at 284.7 eV is attributed to the sp^2 carbon atom, while the peak positioned at 288.8 eV is assigned to the O=C–OH species. Besides the C1s peak, the O1s peak was obtained at 530.1 eV in Fig. 2C. And from Fig. 2D, we also find a dramatic change of the Zn2p peaks at 1021.2 ($Zn2p_{3/2}$) and 1044.3 eV ($Zn2p_{5/2}$). According to the quantitative analysis of the XPS data, the corresponding molar percentages of C, O, Zn species were carried out, and the Zn/C and O/C ratios were obtained by calculation of peak area. And, ratios of 28.6 and 7.9 correspond to Zn/C and O/C, respectively.

3.1.3. *Ultraviolet (UV) and photoluminescence (PL) characterization of ZnO nanosphere and ZnO/G composite*

UV–vis absorption spectra of pure ZnO and ZnO/G composite were shown in Fig. 3A. The sharp characteristic absorption peak at 363 nm indicated the presence of good crystalline and impurity suppressed ZnO nanostructures. The presence of graphene induced an obvious increasement for light absorption intensity, which may be due to an increase of the surface electric charge of the oxides in the ZnO/G composite and modification of the fundamental process of electron–hole pair formation during irradiation (Xu et al., 2011). Additionally a red shift in the absorption peak (from 363 nm to 367 nm) was observed when GO was added to form the ZnO/G composite, which was ascribed to the chemical bonding between the semiconductor photocatalyst and graphene. This was similar to the result in the case of TiO_2-graphene composite materials (Zhang et al., 2010a, 2010b). ZnO/G composite was exposed to UV irradiation produced by a 500 W high pressure Hg lamp with the main wave crest at 365 nm, so ZnO/G could be irradiated well to produce PEC signal with an absorption peak at 367 nm. PL spectra of ZnO naospheres and ZnO/G composite were reported in Fig. 3B. ZnO nanospheres showed a

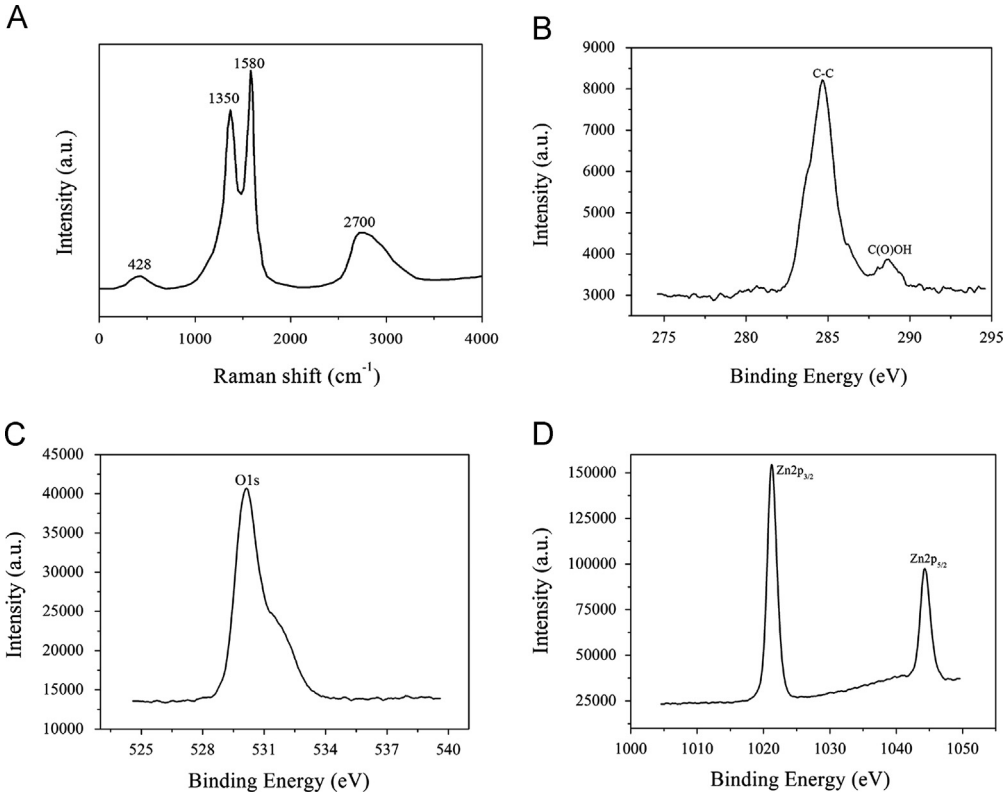

Fig. 2. Raman spectra of ZnO/G (A); XPS spectra of ZnO/G: C1s (B); O1s (C); Zn2p (D).

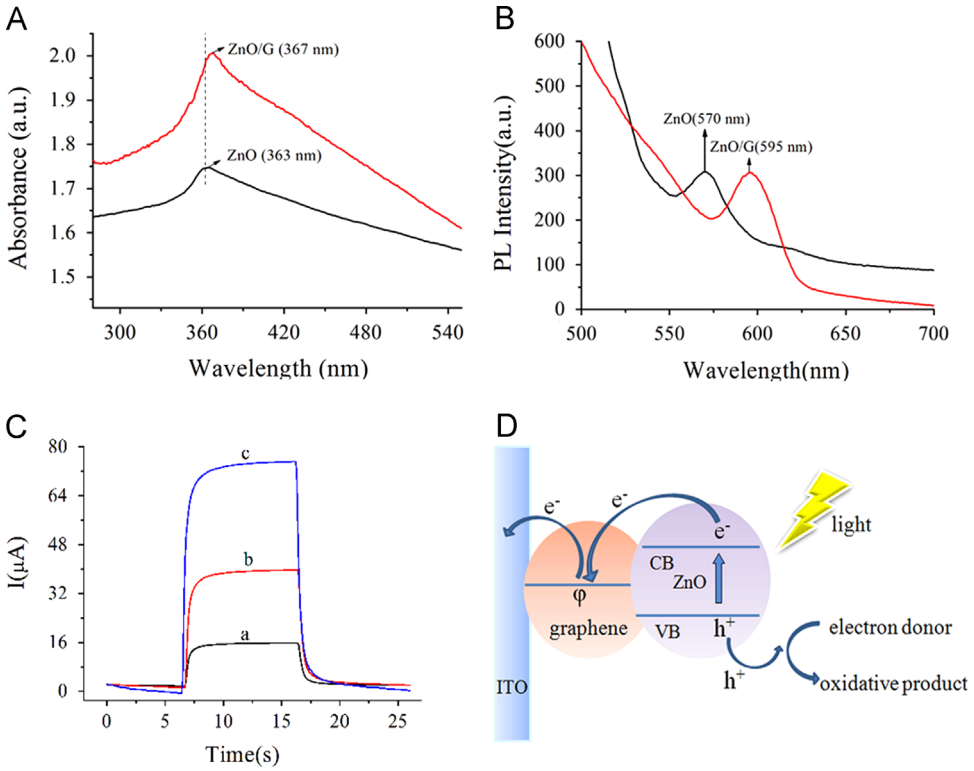

Fig. 3. UV–vis absorption spectra (A) and PL spectra (B) of the ZnO nanosphere and ZnO/G composite; photocurrent responses of ZnO and ZnO/G modified ITO WE (C); photocurrent generation mechanism of ZnO/G (D), CB, VB and φ are the conduction band, valence band, and work function, respectively. UV-light illumination: λ=365 nm; electrolyte: 0.1 M AA aqueous solution; electrode potential of 0 V.

weak emission at 570 nm, whereas ZnO/G composite showed a relatively intense emission centered at 595 nm. The emission band shift in the PL spectrum could be attributed to the interaction between ZnO and graphene. As a conclusion, the UV–vis absorption spectra and PL spectra both indicated the successful preparation of ZnO/G composite.

3.2. Possible mechanism for the PEC performance enhancement of the ZnO/G composite

Fig. 3C showed the photocurrent responses for different nanoparticals. The photocurrent of hollow ZnO nanospheres exhibited a great enhancement compared with cubic ZnO (see Fig. 2S, in supplemental material) due to the unique hollow structure with larger specific surface area (Kato et al., 2012). The photocurrent of ZnO/G composite showed twice the intensity than that of pure ZnO, which can be explained as follows. On one hand, the presence of graphene in ZnO increases the light absorption intensity, which resulted in the enhancement for the photocatalytic performance. On the other hand, the photogenerated electrons would transfer from the conduction band of ZnO to graphene, and the graphene could serve as an acceptor of electrons and suppress charge recombination effectively, resulting in higher photocurrent density.

Another mechanism responsible for the photocatalytic performance is the stepwise structure of energy levels constructed in the ZnO/G composite, as shown in Fig. 3D. The conduction band of ZnO is −4.05 eV (vs. vacuum) and valence band is −7.25 eV (vs. vacuum) (Li and Cao, 2011). The work function of graphene is −4.42 eV (Yang et al., 2010b). On the basis of the relevant band positions of ZnO and graphene, the photogenerated electrons would easily transfer from the conduction band of ZnO to graphene, thus improving the PEC performance. Then the electron transfered to the ITO electrode and the hole could be captured by an electron donor (or hole scavenger) presented in AA solution, resulting the generation of photocurrent.

3.3. Electrochemical impedance spectra (EIS) characterization of the PEC biosensor

As an effective tool for characterizing the interface properties of electrodes, EIS was applied to probe the biosensor fabrication process using $K_3Fe(CN)_6/K_4Fe(CN)_6$ as a redox probe. Fig. 4A displayed the Nyquist diagrams of each electrode involving different construction step of the PEC biosensor. The probe showed a low electron-transfer resistance (R_{et}) at a bare ITO electrode (curve a). After ZnO/G was drop-cast onto the surface of ITO WE, R_{et} decreased to a large extent (curve b), because ZnO is a good electron acceptor with high electron mobility (Chou et al., 2007) and graphene could greatly facilitate the electron transfer. Subsequently, AuNPs and S6 aptamers (curve c) were modified on the surface of ZnO/G, resulting in the increase of R_{et}. Then, BSA (curve d) and SK-BR-3 breast cancer cells (curve e) were constructed step by step, and the R_{et} of each related electrode increased correspondingly. The elevating hindrance effect and insulating effect introduced by biological materials suggested successful stepwise fabrication of the proposed biosensor.

The fabrication of the cell sensor could also be monitored by PEC experiments and was shown in Fig. 4B. The bared ITO electrode showed nearly zero photocurrent (curve a). After ZnO/G was drop-cast onto a bare ITO WE surface, the photocurrent intensity increased significantly (curve b). This demonstrated that ZnO/G composite was a great choice for the construction of a PEC biosensor, due to its cooperative effect for the enhancement of the PEC performance. Subsequently, the photocurrent intensity decreased after immobilization of AuNPs and S6 aptamers (curve c). After BSA (curve d) and SK-BR-3 breast cancer cells (curve e) were immobilized, the photocurrent signal decreased gradually. This

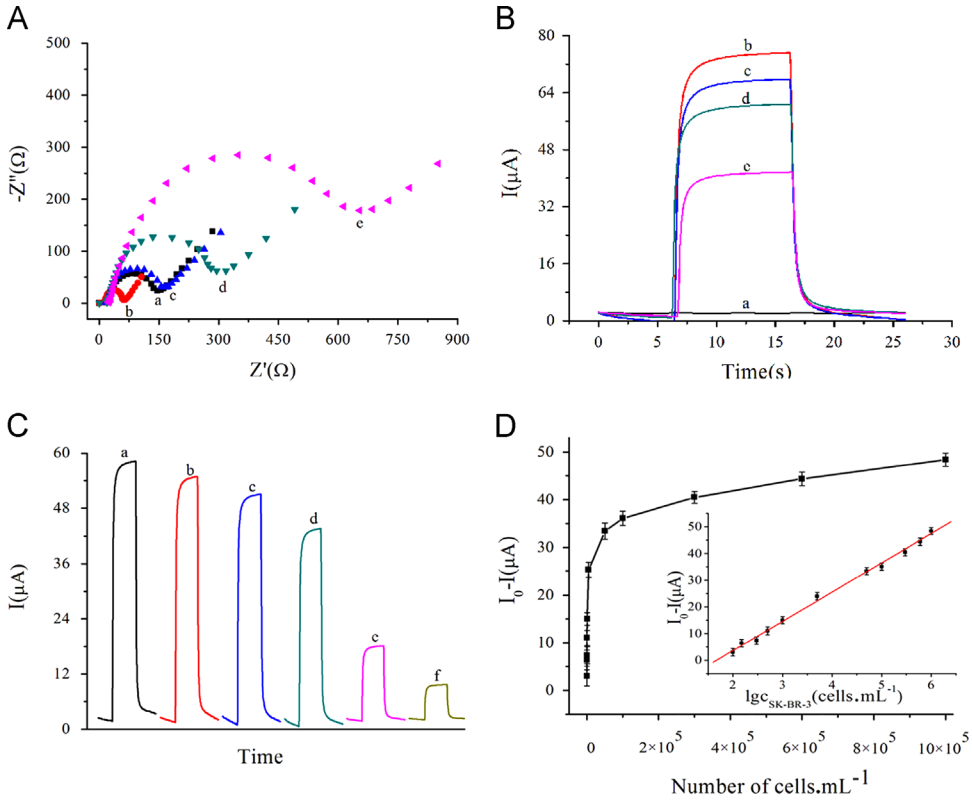

Fig. 4. Nyquist plots of EIS (A) and corresponding photocurrent responses of the modified ITO electrode (B); photocurrent signals of this cell sensor incubated with different concentrations (cells mL^{-1}) of SK-BR-3 cell (a: 0, b: 1×10^2, c: 3×10^2, d: 1×10^3, e: 3×10^5, f: 1×10^6) (C); relationship between ΔI (I_0–I) and SK-BR-3 cells concentration, each point is the average of five measurements (Inset: logarithmic calibration curve for SK-BR-3 cells) (D).

could be explained by the fact that the immobilization of these organic materials on the ITO electrode increased the barrier for the diffusion of AA to the surface of ZnO nanospheres, which would induce the decrease of the photocurrent.

3.4. Sensitive PEC detection of SK-BR-3 breast cancer cells

Fig. 4C showed the PEC intensity of the cell sensor in the absence (a: I_0) and presence (b–f: I) of different concentrations of SK-BR-3 cancer cells. The photocurrent–time curve clearly illustrated the rapid response of the modified electrode to different concentrations of target cells at an applied potential of 0 V with UV light irradiation. From Fig. 4C, it was observed that the PEC intensity decreased gradually with increasing cell concentrations. The reason was that the specific binding of target cells could insulate the conductive support and perturb the interfacial electron transfer and thus decrease the PEC intensity, which suggested that the SK-BR-3 cancer cell concentration could be determined by the PEC measurement of this biosensor.

Under the optimized experimental conditions (see in supplemental material), we explored the quantitative range of the proposed PEC biosensor. The cell sensors were incubated with different concentrations of SK-BR-3 cancer cells. As expected, the ΔI (I_0–I) increased with the increasing concentration of SK-BR-3 cancer cells (Fig. 4D) and the ΔI was linear with the logarithm of cell concentrations in the range of 1×10^2–1×10^6 cells mL^{-1}. The regression equation was $\Delta I = -18.17 + 10.94 \lg (c_{SK\text{-}BR\text{-}3}$, cells $mL^{-1})$, with a correlation coefficient of 0.9972 and a detection limit of 58 cells mL^{-1} (S/N=3). The proposed PEC biosensor exhibited a low detection limit and a wide linear range for cancer cells compared with other methods (Table S1). The improvement of the sensitivity of PEC was attributed to the good performance of the ITO microdevice and the ZnO/G composite, as well as the strong affinity for S6 aptamer to SK-BR-3 cell.

3.5. Specificity, stability, and cytotoxicity of the cell-based biosensor

Usually, nonspecific adsorption is a major problem in label-free biosensing, since it cannot be distinguished from specific adsorption. To confirm that the observed photocurrent changes arised from specific interaction between the S6 aptamers and the SK-BR-3 breast cancer cells, controllable experiments were performed. MCF-7 breast cancer cell was analogous to the target cancer cell, so it was selected as the contrastive cell. Fig. 5A and B showed photographs of SK-BR-3 and MCF-7 cancer cells, respectively. The photocurrent responses of BSA-blocked photoelectrodes in the presence of a PBS solution containing SK-BR-3 cells or MCF-7 cells with different cell concentrations were shown in Fig. 5C. As can be observed, the photocurrent apparently decreased with the increasing concentration of SK-BR-3 cancer cell, but produced no noticeable change with the increasing concentration of MCF-7 cancer cells vs. blank solution without cells (I_0). This suggested that this new cancer cell detection method was highly specific to SK-BR-3 cell. The excellent specificity was due to that S6 aptamer showed strong affinity to SK-BR-3, HER-2-high expressing cancer cell line, but not to MCF-7, HER-2-low expressing cancer cell line, so MCF-7 cell could be easily washed away.

The stability is a vital parameter in the performance of the prepared cell sensor. As shown in Fig. 5D, after the cell sensors were stored in a dry environment at 4 °C for two weeks, the photocurrent value declined 4.65% and 4.10% of the initial response for the prepared biosensor at target cell concentrations of 1×10^3 cells mL^{-1} and 1×10^4 cells mL^{-1}, respectively. The inset in Fig. 5D is the PEC signal-time curve under on and off

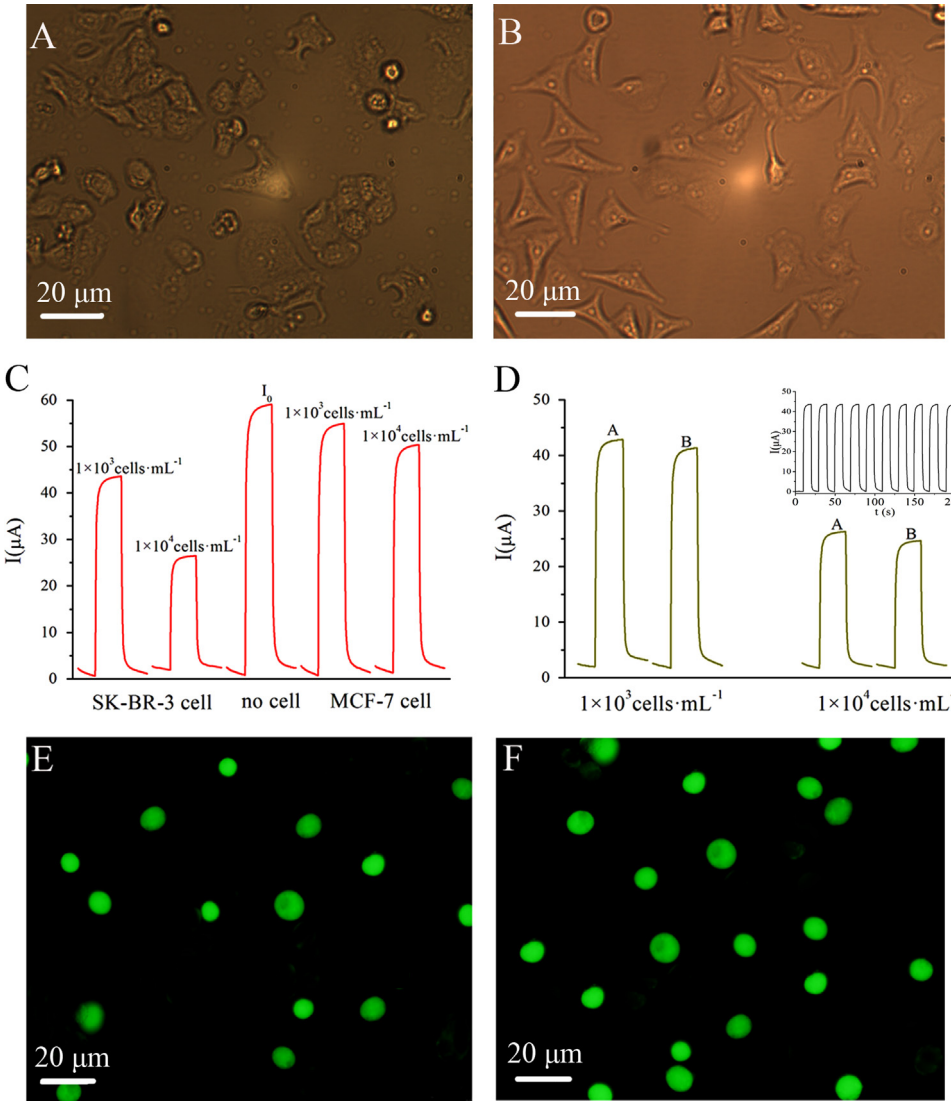

Fig. 5. Photographs of SK-BR-3 (A) and MCF-7 (B) cancer cells; specificity of the cell-based sensor (C); comparison of PEC signals for the first prepared cell sensor (a) and two weeks later (b) recognized with a series of target SK-BR-3 cancer cells for 1×10^3 cells mL^{-1} and 1×10^4 cells mL^{-1}, respectively (the inset was the stabilization of PEC signal of 1×10^3 cells mL^{-1} target SK-Br-3 cells) (D); fluorescent micrographs of SK-BR-3 cells having been incubated with fabricated PEC platforms for 1 h (E) and 4 h (F).

of ultraviolet light irradiation for 10 times. As can be observed, PEC signal declined little. These indicated that the cancer cell sensor had quite acceptable stability, which can be attributed to the excellent stability of ZnO/G composites and ITO microelectrode, and strong interactions between the cells and S6 aptamers modified electrode.

To provide the information on the cytotoxicity of the cell-based sensor, we chose to assess SK-BR-3 cells through optical imaging using calcein as cell stain to characterize the cell viability. SK-BR-3 cells were placed inside a 12-well plate and when cultured for two days, cancer cells were digested by pancreatic enzymes. Subsequently, SK-BR-3 cells were incubated with two fabricated PEC platforms (S6 aptamers-AuNPs dotted ZnO/G modified ITO WEs) for 1 h and 4 h, respectively. Then, SK-BR-3 cells were incubated with calcein solution at 37 °C for 20 min. Fig. 5E and F showed fluorescent micrographs of SK-BR-3 cells and cells having been incubated on modified electrode for 1 h (E) and 4 h (F), respectively. As can be observed, as the incubation time increased, the number of captured cells increased (the green fluorescence indicates viable cells). This result demonstrated that the proposed cell sensor showed no obviously diminishing of the cell viability. The low cytotoxicity of AuNPs dotted ZnO/G composite was related to the properties of the chemically inert, low-cytotoxic raw material (Akhavan et al., 2012c; Mao et al., 2013), which did not release any toxic species.

4. Conclusions

In conclusion, ZnO/G composite and S6 aptamer were applied to the sensitive PEC detection of SK-BR-3 cancer cells based on a disposable ITO microdevice. The proposed cell sensor showed several significant advantages. First, ZnO/G composite was used to trigger and improve PEC performance, due to the high photoelectric activity of ZnO hollow nanospheres and superior charge transportation and separation of graphene. Second, the high specificity of S6 aptamers to target SK-BR-3 cells and the biobarcode technique to avoid cross-reaction were used in the assays, which much favored for the improvement of selectivity and sensitivity. Third, in this approach, ITO-based SPEs device with low-cost acid etch treatment, showed excellent stability for PEC application. These features, as well as excellent biocompatibility, make it a promising candidate for the early and accurate detection of cancer cells.

Acknowledgments

This work was financially supported by Natural Science Research Foundation of China (21277058, 21175058), Natural Science Foundation of Shandong Province, China (ZR2012BZ002, ZR2011BQ019, ZR2011EL029).

Appendix A. Supporting information

Supplementary data associated with this article can be found in the online version at http://dx.doi.org/10.1016/j.bios.2013.07.066.

References

Akhavan, O., 2010. ACS Nano 4, 4174–4180.
Akhavan, O., Ghaderi, E., Rahighi, R., 2012b. ACS Nano 6, 2904–2916.
Akhavan, O., Ghaderia, E., Emamy, H., 2012a. Journal of Materials Chemistry 22, 20626–20633.
Akhavan, O., Ghaderi, E., Akhavan, A., 2012c. Biomaterials 33, 8017–8025.
Akhavan, O., Ghaderia, E., 2013. Small, http://dx.doi.org/10.1002/smll.201203106.
Akhavan, O., 2011. Carbon 49, 11–18.
Chen, Y.L., Hu, Z.A., Chang, Y.Q., Wang, H.W., Zhang, Z.Y., Yang, Y.Y., Wu, H.Y., 2011. Journal of Physical Chemistry C 115, 2563–2571.
Chou, T.P., Zhang, Q.F., Fryxell, G.E., Cao, G.Z., 2007. Advanced Materials 19, 2588–2592.
Cho, S., Jang, J.W., Lee, J.S., Lee, K.H., 2010. CrystEngComm 12, 3929–3935.
Chen, Y.T., Jiang, Y.Y., Lin, Z.Y., Sun, J.J., Zhang, L., Chen, G.N., 2009a. Analyst 134, 731–737.
Chen, X., Estevez, M.C., Zhu, Z., Huang, Y.F., Chen, Y., Wang, L., Tan, W.H., 2009b. Analytical Chemistry 81, 7009–7014.
Calizo, I., Balandin, A.A., Bao, W., Miao, F., Lau, C.N., 2007. Nano Letters 7, 2645–2649.
Ferrari, A.C., Meyer, J.C., Scardaci, V., Casiraghi, C., Lazzeri, M., Mauri, F., Piscanec, S., Jiang, D., Novoselov, K.S., Roth, S., Geim, A.K., 2006. Physical Review Letters 97, 187401.
Faenza, A., Bocchi, M., Pecorari, N., Franchi, E., Guerrieri, R., 2012. Lab on a Chip 12, 2046–2052.
Hu, S.H., Che, Y.W., Hun, W.T., Che, I.W., Chen, S.Y., 2012. Advanced Materials 24, 1748–1754.
Kudin, K.N., Ozbas, B., Schniepp, H.C., Prud'homme, R.K., Aksay, I.A., Car, R., 2008. Nano Letters 8, 36–41.
Krishnamurthy, S., Cristofanilli, M., Singh, B., Reuben, J., Gao, H., Cohen, E.N., Andreopoulou, E., Hall, C.S., Lodhi, A., Jackson, S., Lucci, A., 2010. Cancer 116, 3330–3337.
Kato, M., Cardona, T., Rutherford, A.W., Reisner, E., 2012. Journal of the American Chemical Society 134, 8332–8335.
Kim, K.S., Zhao, Y., Jang, H., Lee, S.Y., Kim, J.M., Kim, K.S., Ahn, J.H., Kim, P., Choi, J.Y., Hong, B.H., 2009. Nature 457, 706–710.
King, S.H., Huh, Y.M., Kim, S., Lee, D.K., 2009. Bulletin of the Korean Chemical Society 30, 1827–1831.
Kavitha, T., Gopalan, A.L., Lee, K.P., Park, S.Y., 2012. Carbon 50, 2994–3000.
Liu, X.J., Pan, L.K., Lv, T., Lu, T., Zhu, G., Sun, Z., Sun, C.Q., 2011. Catalysis Science and Technology 1, 1189–1193.
Luo, Q.P., Yu, X.Y., Lei, B.X., Chen, H.Y., Kuang, D.B., Su, C.Y., 2012. Journal of Physical Chemisrty C 116, 8111–8117.
Li, B., Cao, H., 2011. Journal of Materials Chemistry 21, 3346–3349.
Li, Y.J., Ma, M.J., Zhu, J.J., 2012. Analytical Chemistry 84, 1049–1055.
Meng, S.G., Li, D.Z., Zheng, X.Z., Wang, J.X., Chen, J., Fang, J.L., Shao, Y., Fu, X.Z., 2013. Journal of Materials Chemistry A 1, 2744–2747.
Metters, J.P., Kadara, R.O., Banks, C.E., 2011. Analyst 136, 1067–1076.
Mao, H.Y., Laurent, S., Chen, W., Akhavan, O., Imani, M., Ashkarran, A.A., Mahmoudi, M., 2013. Chemical Reviews 113, 3407–3424.
Markovic, Z.M., Harhaji-Trajkovic, L.M., Todorovic-Markovic, B.M., Kepic, D.P., Arsikin, K.M., Jovanovi, S.P., Pantovic, A.C., Dramicanin, M.D., Trajkovic, V.S., 2011. Biomaterials 32, 1121–1129.
Nam, J., Won, N., Jin, H., Chung, H., Kim, S., 2009. Journal of the American Chemical Society 131, 13639–13645.
Pantel, K., Brakenhoff, R.H., Brandt, B., 2008. Nature Reviews Cancer 8, 329–340.
Robinson, J.T., Tabakman, S.M., Liang, Y.Y., Wang, H.L., Casalongue, H.S., Vinh, D., Dai, H.J., 2011. Journal of the American Chemical Society 133, 6825–6831.
Shen, Q.M., Zhao, X.M., Zhou, S.W., Hou, W.H., Zhu, J.J., 2011. Journal of Physical Chemistry C 115, 17958–17964.
Stefano, L.D., Rea, I., Armenante, A., Giardina, P., Giocondo, M., Rendina, I., 2007. Langmuir 23, 7920–7922.
Tian, J.Q., Liu, S., Li, H.Y., Wang, L., Zhang, Y.W., Luo, Y.L., Asiri, A., Al-Youbi, A.O., Su, X.P., 2012. RSC Advances 2, 1318–1321.
Tang, L.H., Wang, Y., Li, Y.M., Feng, H.B., Lu, J., Li, J.H., 2009. Advanced Functional Materials 19, 2782–2789.
Wu, C.X., Li, F.S., Zhang, Y.G., Guo, T.L., 2012. Carbon 50, 3622–3626.
Xu, T.G., Zhang, L.W., Cheng, H.Y., Zhu, Y.F., 2011. Applied Catalysis B. Environmental 101, 382–387.
Yang, K., Wan, J.M., Zhang, S., Tian, B., Zhang, Y.J., Liu, Z., 2011. Biomaterials 33, 2206–2214.
Yang, N.L., Zhai, J., Wang, D., Chen, Y.S., Jiang, L., 2010a. ACS Nano 4, 887–894.
Yang, K., Hu, L.L., Ma, X.X., Ye, S.Q., Cheng, L., Shi, X.Z., Li, C.H., Li, Y.G., Liu, Z., 2012. Advanced Materials 24, 1868–1872.
Yang, K., Zhang, S., Zhang, G.X., Sun, X.M., Lee, S.T., Liu, Z., 2010b. Nano Letters 10, 3318–3323.
Zhang, Y.H., Tang, Z.R., Fu, X.Z., Xu, Y.J., 2010b. ACS Nano 4, 7303–7314.
Zhang, W., Guo, Z.,Y., Huang, D.Q., Liu, Z.M., Guo, X., Zhong, H.Q., 2011. Biomaterials 32, 8555–8561.
Zhang, Q.F., Chou, T.P., Russo, B., Jenekhe, S.A., Cao, G.Z., 2008. Angewandte Chemie International Edition 47, 2402–2406.
Zhang, L.W., Cheng, H.Y., Zong, R.L., Zhu, Y.F., 2009. Journal of Physical Chemistry C 113, 2368–2374.
Zhao, W.W., Tian, C.Y., Xu, J.J., Chen, H.Y., 2012. Chemical Communications 48, 895–897.
Zhang, H., Lv, X.J., Li, Y.M., Wang, Y., Li, J.H., 2010a. ACS Nano 4, 380–386.